International Journal of Applied Mathematics
Volume 38 No. 8s, 2025
ISSN: 1311-1728 (printed version); ISSN: 1314-8060 (on-line version)

ADAPTIVE MULTICHANNEL SIGNAL DECOMPOSITION FOR IMPROVED NEURAL ACTIVITY INTERPRETATION IN COGNITIVE NEUROSCIENCE

Dr. Aniruddha Deka[1*], Azharul Alom[2]

[1*]Associate Professor, Program of Computer Science and Engineering, Faculty of Computer Technology, Assam down town University
Email ID: aniruddha.deka@adtu.in
[2]Student, Program of Computer Science and Engineering, Faculty of Computer Technology
Assam down town University
Email ID: alom.azhar@gmail.com

Abstract: Accurate analysis of multichannel brain signals such as EEG is crucial in neuroscience, yet it remains challenging due to their nonstationary and noise-prone nature. Multivariate Mode Decomposition (MMD) offers a mathematically grounded approach for signal decomposition but relies on fixed, manually tuned parameters—specifically, the number of modes (ρ) and the penalty factor (α). Improper selection of these parameters can lead to mode mixing, information loss, and reduced interpretability, limiting its effectiveness in cognitive and clinical neuroscience. To address these limitations, we propose a Self-Adaptive Multivariate Mode Decomposition (SAMMD) algorithm that dynamically adjusts ρ and α during decomposition. Inspired by the matching pursuit strategy and based on frequency-domain orthogonality, SAMMD adaptively extracts oscillatory components sequentially, aligning effectively with the time–frequency complexity of neural signals. Experimental results on both synthetic and real-world datasets, including EEG alpha rhythm extraction and plant-wide control system oscillation detection, demonstrate that SAMMD achieves superior mode alignment, improved noise robustness, and strong resilience to parameter sensitivity. Compared with MMD, MEMD, and Fast MEMD, SAMMD yields the lowest decomposition error and the most consistent spectral separation. The findings highlight SAMMD's potential as a powerful tool for precise and adaptive brain signal decomposition, thereby advancing neuroscientific insights into neural oscillations and brain dynamics.

Keywords: Multivariate Mode Decomposition; Brain Signal Analysis; EEG Signal Processing; Neuroscience; Signal Decomposition; Cognitive Neuroscience.

I. Introduction

The human brain generates complex, nonstationary signals that capture dynamic neural processes across multiple temporal and spatial scales. **Electroencephalography (EEG)**, **magnetoencephalography (MEG)** [1], and other neurophysiological modalities are extensively employed in neuroscience to investigate cognitive functions, neural oscillations, and pathological brain activity. However, these signals are often affected by noise and consist of overlapping frequency components, thereby making accurate signal decomposition essential for extracting meaningful and reliable neural information. Traditional decomposition methods often struggle with mode mixing and parameter sensitivity [2], limiting their effectiveness in identifying distinct brain rhythms such as alpha, beta, or gamma waves. Therefore, there is a critical need for adaptive signal processing techniques that can robustly separate neural components in a data-driven manner. This study addresses this need by proposing a self-adaptive multivariate decomposition framework tailored for brain signal analysis, enhancing the interpretability and reliability of neural oscillatory patterns in cognitive and clinical neuroscience [3-4].

Signal decomposition method is directly applied to each channel of a multivariate signal one by one; it not only ignores the inter-channel correlation information but also fails to ensure mode alignment [5]. The development of multivariate signal decomposition techniques originated with the **Complex**

Received: August 02, 2025

International Journal of Applied Mathematics
Volume 38 No. 8s, 2025
ISSN: 1311-1728 (printed version); ISSN: 1314-8060 (on-line version)

Empirical Mode Decomposition (CEMD). As reported in [6], CEMD was initially proposed to analyze complex-valued signals; however, its applicability was limited due to its inability to process real multichannel data. Subsequently, the author in [7] introduced the **Bivariate Empirical Mode Decomposition (BEMD)**, which explicitly defined extrema, mean, and envelopes of bivariate signals in a three-dimensional space. Building upon this framework, **Rehman and Mandic** [8,9] extended BEMD to formulate the **Trivariate EMD (TEMD)** and the more generalized **Multivariate EMD (MEMD)**.

Since its introduction, the **Multivariate Empirical Mode Decomposition (MEMD)** algorithm has attracted considerable attention and has been extensively applied across various domains, including **biomedicine** [10], **process control** [11], and **geophysics** [12]. However, the computational complexity of MEMD increases substantially with the number of signal channels. To mitigate this limitation, the author in [13] introduced the **Fast MEMD (FMEMD)** algorithm. By establishing the interchangeability between multivariate signal projection and decomposition, the approach transforms the multivariate spline interpolation problem inherent in MEMD into a univariate one, thereby significantly improving computational efficiency. Despite the advantages inherited from EMD, these multivariate decomposition techniques still exhibit certain drawbacks, such as sensitivity to sampling frequency, limited noise robustness, and the absence of rigorous mathematical foundations [14–16].

Compared with **Multivariate Empirical Mode Decomposition (MEMD)**, the **Multivariate Mode Decomposition (MMD)** demonstrates superior noise robustness and stronger resistance to mode mixing. Due to these advantageous characteristics, MMD has been effectively applied in several domains, including **EEG signal detection** [17], **wind turbine fault diagnosis** [18], and **signal denoising** [19]. However, as a completely non-recursive decomposition model, the performance of MMD is highly dependent on two preset parameters: the number of modes (ρ) and the penalty factor (α). An inappropriate selection of ρ may lead to mode loss or mode mixing, while the choice of α significantly affects the quality of decomposition. Moreover, MMD provides no explicit guideline for determining the optimal value of α, thereby limiting its adaptability and generalization in practical scenarios. To overcome these limitations and enhance the practical applicability of the MMD algorithm, this study proposes a **Self-Adaptive Multivariate Mode Decomposition (SAMMD)** approach.

This study introduces a novel self-adaptive signal decomposition framework, **SAMMD**, specifically designed to improve the analysis of multichannel brain signals in neuroscience. The key contributions of this work are summarized as follows:

1. **Development of a Self-Adaptive MMD Framework:** A recursive decomposition strategy is proposed, inspired by matching pursuit, that adaptively determines the number of modes (ρ) and dynamically updates the penalty factor (α) during the optimization process, eliminating the need for manual parameter tuning.

2. **Bandwidth Adaptation via Mode Orthogonality:** A novel penalty factor update rule based on frequency-domain orthogonality ensures that the bandwidth of each mode narrows progressively, improving noise suppression and preserving signal integrity particularly beneficial for capturing neural oscillations.

3. **Improved Mode Alignment and Noise Robustness:** SAMMD demonstrates superior performance in separating overlapping frequency components in multichannel EEG signals,

Received: August 02, 2025

International Journal of Applied Mathematics
Volume 38 No. 8s, 2025
ISSN: 1311-1728 (printed version); ISSN: 1314-8060 (on-line version)

achieving better mode alignment and resilience to noise compared to MMD, MEMD, and Fast MEMD.

The structure of this paper is as follows: Section 2 provides a detailed introduction to the objective function and algorithmic flow of SAMMD; Section 3 studies the characteristics of SAMMD, including filter bank structure, robustness to noise, and variations in the α value, and verifies the effectiveness and superiority of the algorithm through a simulation case; Section 4 further demonstrates the practicality of the algorithm with two real-world case studies; Section 5 summarizes the full text and offers prospects for future work.

II. Self-Adaptive MMD Decomposition

MMD inherits many ideal properties of standard VMD, such as having a good mathematical framework and avoiding endpoint effects in the process of solving multivariate modulated oscillations through the mirror extension method. However, MMD still has the following shortcomings: (1) It is necessary to specify the number of modes ρ in advance. In practical applications, the inherent number of modes in complex signals is difficult to predict. If ρ is set improperly, it may cause problems such as over-decomposition or under-decomposition. (2) The penalty factor α is fixed. From the mode update formula of MMD, it can be seen that the size of α determines the bandwidth of the mode. In the early stage of optimization, a relatively wide filter bandwidth is needed to capture the correct centre mode, while in the later stage of optimization, the obtained mode is already near the expected value, and at this time, a narrower bandwidth is needed to filter out noise and other interference factors [20,21]. Therefore, updating the value of α during the optimization process is more reasonable.

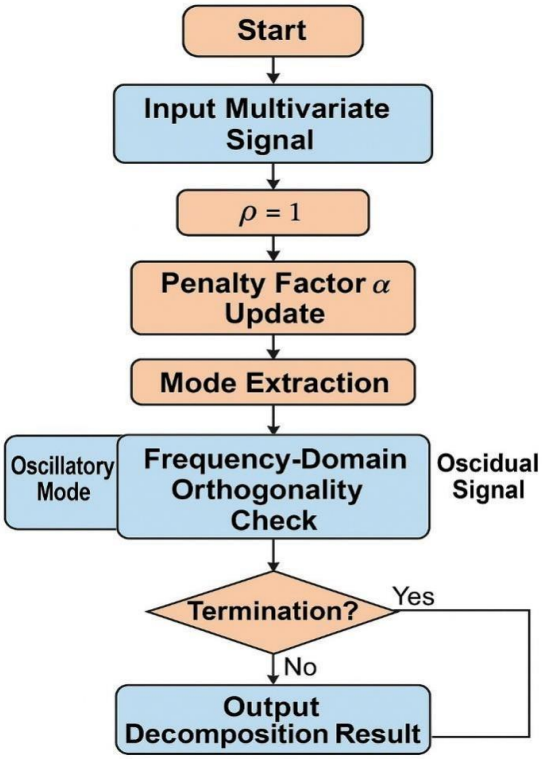

Figure 1: Framework for Self-Adaptive MMD Decomposition

To solve the above parameter tuning problem, inspired by recent related work [20,21], this paper proposes the SAMMD algorithm. This algorithm improves the original MMD objective function and changes the joint optimization framework into a recursive framework. Specifically, SAMMD extracts

International Journal of Applied Mathematics
Volume 38 No. 8s, 2025
ISSN: 1311-1728 (printed version); ISSN: 1314-8060 (on-line version)

multivariate modulated oscillations one by one, rather than extracting them simultaneously. The number of modes ρ is determined by the energy proportion of the residual signal and does not need to be specified in advance. In addition, the SAMMD algorithm proposes a bandwidth updating rule based on mode orthogonality, so that the bandwidth of the mode continuously adjusts during the optimization process. This section will introduce the proposed SAMMD algorithm in detail from two aspects: objective function and specific steps.

2.1 Objective Function

MMD minimizes the sum of the bandwidths of all channels and all modes, while SAMMD minimizes the sum of the bandwidths of the modes at each layer/each scale to construct a variational optimization problem.

$$\underset{\{v_{\rho,c}\},\{\beta_\rho\}}{\text{minimize}} \left\{ \alpha \sum_c \left\| \partial_t \left[v_{\rho,c}^{+}(t) \mathrm{e}^{-\mathrm{j}\beta_\rho t} \right] \right\|_2^2 + \sum_c \left\| x_c(t) - v_{\rho,c}(t) \right\|_2^2 \right\} \tag{1}$$

Where the subscripts ρ and c are used for mode and channel counting, $x_c\,(t)$ is the signal corresponding to each channel, and α is the penalty factor. SAMMD adopts the idea of the Wiener filter; the first term in Equation (1) adds a smoothness constraint to the mode $v_{\rho,c}\,(t)$,representing the sum of the bandwidths of the modes of all channels at each layer, and the second term represents the sum of the residual signals in each channel. According to the Alternating Direction Method of Multipliers, the above complex optimization problem can be transformed into two sub-optimization problems, that is, alternately updating the mode and the center frequency. At the same time, according to the orthogonality between the mode and the residual signal in the frequency domain, an update formula for the penalty coefficient α can be derived. The derivation process of updating $v_{\rho,c}\,(t)$, β_ρ and α is as follows.

2.1.1 Update of mode $\mathbf{v}_{k,c}\,(t)$

$$v_{\rho,c}^{n+1} = \arg\min_{v_{\rho,c}} \left\{ \alpha \left\| \partial_t \left[v_{\rho,c}^{+}(t) \mathrm{e}^{-\mathrm{j}\beta_\rho t} \right] \right\|_2^2 + \left\| x_c(t) - v_{\rho,c}(t) \right\|_2^2 \right\} \tag{2}$$

After transforming to the frequency domain:

$$v_{\rho,c}^{n+1}(\beta) = \arg\min \left\{ \alpha \left\| \mathrm{j}\beta \left[\left(1 + \mathrm{sgn}(\beta + \beta_\rho)\right) \cdot v_{\rho,c}(\beta + \beta_\rho) \right] \right\|_2^2 + \left\| x_c(\beta) - v_{\rho,c}(\beta) \right\|_2^2 \right\} \tag{3}$$

Removing the L2 norm in Equation (3), then taking the partial derivative of the right-hand side with respect to $u_k,c(\omega)$ and rearranging yields:

$$v_{\rho,c}^{n+1}(\beta) = \frac{x_c(\beta)}{1+2\alpha\left(\beta-\beta_\rho\right)^2} \tag{4}$$

2.1.2 Update of center frequency ω_k

In Equation (1), only the first term is related to ω_k, so only the first term needs to be focused on during the optimization process.

Received: August 02, 2025

International Journal of Applied Mathematics
Volume 38 No. 8s, 2025
ISSN: 1311-1728 (printed version); ISSN: 1314-8060 (on-line version)

$$\beta_\rho^{n+1} = \arg\min_{\beta_\rho} \left\{ \sum_c \left\| \partial_t \left[v_{\rho,c}^+(t) \mathrm{e}^{-\mathrm{j}\beta_\rho t} \right] \right\|_2^2 \right\} \tag{5}$$

First transform the above equation into the frequency domain, and then remove the L2 norm to obtain:

$$\beta_\rho^{n+1}(\beta) = \arg\min \sum_c \int_0^\infty \left(\beta - \beta_\rho\right)^2 \left| v_{\rho,c}(\beta) \right|^2 \mathrm{d}\beta \tag{6}$$

Take the partial derivative of the right-hand side of Equation (6) with respect to ω_k, and set the derivative to 0.

After rearrangement, the result is obtained.

$$\beta_\rho^{n+1} \leftarrow \frac{\sum_c \int_0^\infty \beta \left| v_{\rho,c}^{n+1}(\beta) \right|^2 \mathrm{d}\beta}{\sum_c \int_0^\infty \left| v_{\rho,c}^{n+1}(\beta) \right|^2 \mathrm{d}\beta} \tag{7}$$

2.1.3 Update of Penalty Coefficient α

After two signals that are orthogonal in the time domain are each transformed into the frequency domain, they remain orthogonal, so it can be known that $v_{\rho^*,c}(\beta) r_{\rho,c}(\beta) = 0$. At the same time, combining $x_c(\beta) = v_{\rho,c}(\beta) + r_{\rho,c}(\beta)$ yields:

$$\frac{v_{\rho,c}^*(\beta) v_{\rho,c}(\beta)}{v_{\rho,c}^*(\beta) x_c(\beta)} = 1 \tag{8}$$

Substituting the update formula of $v_{\rho,c}(\beta)$, i.e., Equation (4), into Equation (8) and rearranging gives:

$$\alpha = \frac{x_c^*(\beta) \left(\frac{1}{1/\alpha + 2(\beta - \beta_\rho)^2} \right)^* \left(\frac{1}{1/\alpha + 2(\beta - \beta_\rho)^2} \right) x_c(\beta)}{x_c^*(\beta) \left(\frac{1}{1/\alpha + 2(\beta - \beta_\rho)^2} \right)^* x_c(\beta)} \tag{9}$$

Since , $\frac{1}{1/\alpha^n + 2\left(\beta - \beta_\rho^n\right)^2} = \alpha^n \frac{1}{1 + 2\alpha^n \left(\beta - \beta_\rho^n\right)^2}$ equation (9) can be expressed as:

$$\alpha^{n+1} = \frac{\alpha^n \left(\frac{x_c(\beta)}{1 + 2\alpha^n \left(\beta - \beta_\rho^n\right)^2} \right)^* \left(\frac{x_c(\beta)}{1 + 2\alpha^n \left(\beta - \beta_\rho^n\right)^2} \right)}{\left(\frac{x_c(\beta)}{1 + 2\alpha^n \left(\beta - \beta_\rho^n\right)^2} \right)^* x_c(\beta)} \tag{10}$$

Substituting equation (4) into equation (10), we get

$$\alpha_c^{n+1} = \alpha_c^n \frac{v_{\rho,c}^{n+1}(\beta)^* v_{\rho,c}^{n+1}(\beta)}{v_{\rho,c}^{n+1}(\beta)^* r_{\rho,c}(\beta)} \tag{11}$$

As the mode $v_{\rho,c}(\beta)$ is continuously updated, the value of the denominator in Equation (11) will gradually decrease, causing the value of α to gradually increase. Consequently, the bandwidth of the

International Journal of Applied Mathematics
Volume 38 No. 8s, 2025
ISSN: 1311-1728 (printed version); ISSN: 1314-8060 (on-line version)

mode continuously decreases during the update process, meeting the previously mentioned requirement for bandwidth updating.

2.2 SAMMD Algorithm

The SAMMD algorithm contains two layers of loops. The outer loop controls the number of modes ρ based on the energy proportion of the residual signal. The termination parameter δ of the outer loop can be adjusted according to the actual noise level. The inner loop is similar to MMD and mainly updates the mode, centre frequency, and α value. The detailed SAMMD algorithm is shown in Algorithm 1.

Algorithm 1 SAMMD algorithm

Initialization : $\{v_{\rho,c}^1(\beta)\},\{\beta_\rho^1\},n \leftarrow 0$

make $\rho = 1, \boldsymbol{r}_1(\beta) = \boldsymbol{x}(\beta)$

while $\|\boldsymbol{r}_\rho(\beta)\|_2^2 / \| \boldsymbol{x}(\beta) \|_2^2 > \delta$ do

make $n = 1$, Initialize center frequency$\{\beta_\rho^1\}$

while $\sum_c \frac{\|v_{\rho,c}^n(\beta) - v_{\rho,c}^{n-1}(\beta)\|_2^2}{\|v_{\rho,c}^{n-1}(\beta)\|_2^2} > \varepsilon$ do

$n \leftarrow n + 1$

for $c = 1: C$ do

$v_{\rho,c}^{n+1}(\beta) \leftarrow \frac{r_{\rho,c}(\beta)}{1+2\alpha_c^n(\beta-\beta_\rho^n)^2}$

end for

$\beta_\rho^{n+1} \leftarrow \frac{\sum_c \int_0^\infty \beta |v_{\rho,c}^{n+1}(\beta)|^2 \, d\beta}{\sum_c \int_0^\infty |v_{\rho,c}^{n+1}(\beta)|^2 \, d\beta}$

for $c = 1: C$ do

$\alpha_c^{n+1} = \alpha_c^n \frac{v_{\rho,c}^{n+1}(\beta)^* v_{\rho,c}^{n+1}(\beta)}{v_{\rho,c}^{n+1}(\beta)^* r_{\rho,c}(\beta)}$

end for

make $v_{\rho,c}(\beta) = v_{\rho,c}^{n+1}(\beta), \beta_\rho = \beta_\rho^{n+1}$,

Update at the same time $\boldsymbol{r}_{\rho+1}(\beta) = \boldsymbol{x}(\beta) - \boldsymbol{u}_\rho(\beta)$

end while

III. Experimental Detail and Result Analysis

To evaluate the effectiveness of the proposed Self-Adaptive Multivariate Variation Mode Decomposition (SAMMD) algorithm, a comprehensive set of experiments was conducted on both simulated signals and real-world datasets. In the simulation study, classical multivariate signals were generated, consisting of two cosine components with additive Gaussian white noise. These signals are commonly used to benchmark decomposition algorithms due to their known frequency content and controllable noise levels. The signals were sampled at 1000 Hz with a length of 1000 samples, and the noise standard deviation was varied from 0 to 0.5 in steps of 0.1. The initial penalty factor α

Received: August 02, 2025

International Journal of Applied Mathematics
Volume 38 No. 8s, 2025
ISSN: 1311-1728 (printed version); ISSN: 1314-8060 (on-line version)

was set to 1000, and for comparison purposes, the number of modes ρ in MMD was fixed at 2. The accuracy and robustness of SAMMD were evaluated by measuring the deviation of the estimated center frequencies and using the Sum of Absolute Differences (SAD) between the decomposed and ground truth modes. Additionally, the power spectral density (PSD) across 100 repeated trials was analyzed to evaluate filter bank consistency.

To further demonstrate the practical value of SAMMD, two real-world case studies were conducted. The first involved electroencephalogram (EEG) signal analysis using a 4-channel dataset recorded during an eyes-closed resting state. SAMMD successfully extracted the expected alpha rhythm (8–12 Hz) and correctly identified power-line interference at 50 Hz, whereas MMD showed a frequency shift, misrepresenting the actual artifact. The second case study focused on plant-wide oscillation detection in a mineral processing flotation circuit. Data from nine measurement units were analyzed using SAMMD, and oscillatory components were identified using the normalized correlation coefficient and the Sparsity Index (SI), with modes exhibiting SI values above 0.58 17
considered oscillatory. The results confirmed SAMMD's ability to accurately localize oscillatory behavior across channels, consistent with prior domain knowledge.

All experiments were implemented in Python (and MATLAB where necessary) and run on a workstation with a multi-core CPU. The results clearly show that SAMMD provides superior decomposition performance compared classical methods like MMD, MEMD, and Fast MEMD, particularly in terms of mode alignment, robustness to noise, and adaptability to parameter variations.

3.1 Filter Bank Structure

The filter bank structure is an important characteristic of signal decomposition methods. Many multivariate signal decomposition algorithms analyse the characteristics of their filter banks. Studies have been conducted on this, such as MEMD and MMD [5,22]. By analogy with MEMD and MMD, this section analyses this characteristic of the SAMMD algorithm and compares it with the results of MMD.

A four-channel Gaussian white noise process with a data length of N = 1024 (following a normal distribution with mean 0 and standard deviation σ) is decomposed using SAMMD. To eliminate random factors, the experiment is repeated 100 times, and MMD is also applied to the same dataset. For ease of comparison, the number of modes ρ for both MMD and SAMMD is uniformly set to 8. The average Power Spectral Density (PSD) of both under 100 experiments is shown in Figure 2.

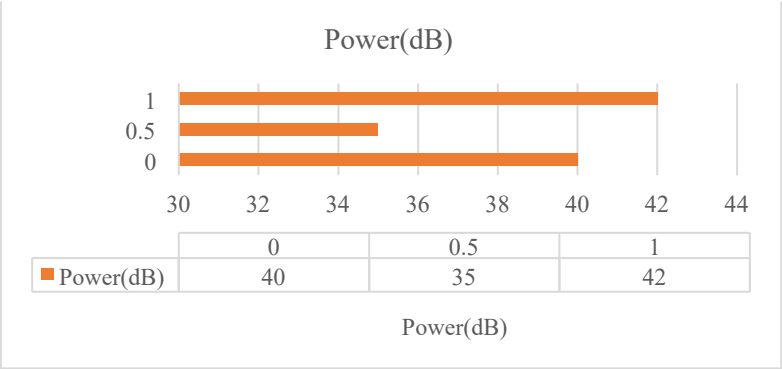

(a) MMD

International Journal of Applied Mathematics
Volume 38 No. 8s, 2025
ISSN: 1311-1728 (printed version); ISSN: 1314-8060 (on-line version)

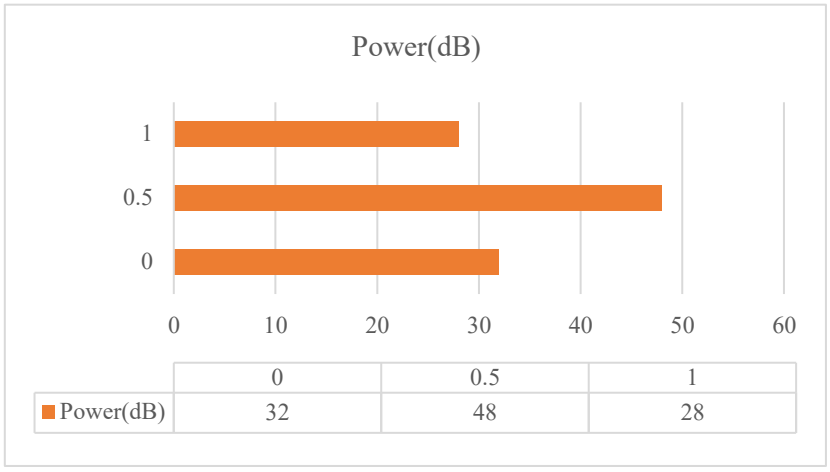

(b) SAMMD

Figure 2: Filter Bank Characteristics

It can be seen that the essence of both algorithms is a set of Wiener filters. Comparing the filter bank characteristics of the two, MMD exhibits obvious overlap between adjacent filters, whereas SAMMD has almost no overlap. According to literature [23], the larger the overlap area between modal spectra, the higher the probability of mode mixing. Therefore, SAMMD has better anti-mode-mixing capability.

3.2 Robustness to Noise and α Value Variation

To investigate the robustness of the SAMMD algorithm with respect to noise and changes in the α value, this section tests SAMMD using a set of classical multivariate signals, as shown in Equation (12). This signal is often used for simulation experiment analysis [1,5,20]. The signal is composed of complex multicomponent, making it well-suited for testing the algorithm's mode alignment and noise robustness.

$$\begin{aligned} \boldsymbol{X}_1(t) &= [x_1(t), x_2(t), x_3(t)] \\ x_1(t) &= (1 + 0.5\cos(2\pi \times t))\cos(2\pi \times 5t) \\ &\quad +\cos(2\pi \times 15t) + z(t) \\ x_2(t) &= \cos(2\pi \times t)\cos(2\pi \times 5t) + \cos(2\pi \times 15t) \\ &\quad +z(t) \\ x_3(t) &= 2\cos(2\pi \times 15t) + z(t) \end{aligned} \tag{12}$$

Where t varies from 0 to 1, the sampling frequency is 1000 Hz, and the signal length is N = 1000. $z(t)$is Gaussian white noise, following a normal distribution $z(t) \sim \mathcal{N}(0, \sigma^2)$. For a fair comparison, the initial value of α for both MMD and SAMMD is set to 1000 (which is the default value in reference [5]), and the number of modes for MMD is set to ρ = 2. Let the standard deviation σ of the Gaussian white noise vary from 0 to 0.5 in intervals of 0.1. The robustness of both algorithms to noise is judged by observing the convergence of the frequencies of the two cosine components. The results are averaged over 100 experiments, as shown in Figure 3(a) and Figure 3(b). It can be seen that as the noise level gradually increases; the final converged centre frequency obtained by SAMMD is closer to its true value. In contrast, the centre frequency of the first mode obtained by MMD when decomposing signal $\boldsymbol{X}1\ (t)$ deviates from the correct value.

Next, the robustness of MMD and SAMMD to changes in the value is discussed. Without loss of generality, the standard deviation of the noise in signal $X_1\ (t)$ is fixed at 0.1, while α is varied from 1

Received: August 02, 2025

International Journal of Applied Mathematics
Volume 38 No. 8s, 2025
ISSN: 1311-1728 (printed version); ISSN: 1314-8060 (on-line version)

to 10,000 with an interval of 1. The effect of different **α** values on the decomposition results of MMD and SAMMD is shown in Figure 3(c) and Figure 3(d). It can be seen that the centre frequency finally converged by SAMMD almost coincides with the correct centre frequency. This is because the α in the SAMMD algorithm has Self-Adaptive capability and gradually adjusts to a suitable value during the update process, thereby ensuring the accuracy of the decomposition. In contrast, MMD 's convergence curve does not reach the expected result and is more sensitive to the value of the parameter **α**.

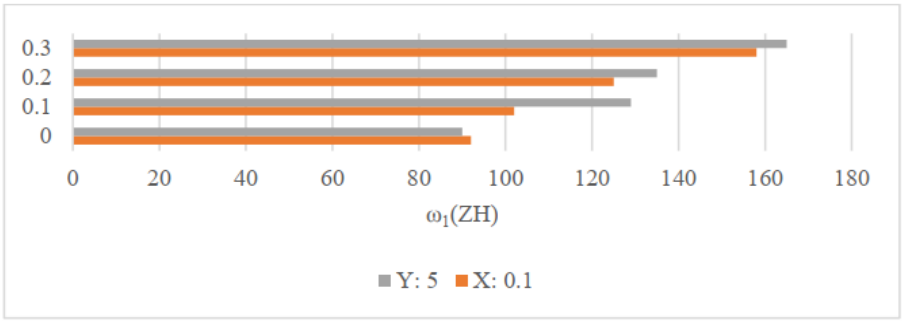

(a) Noise robustness of mode 1

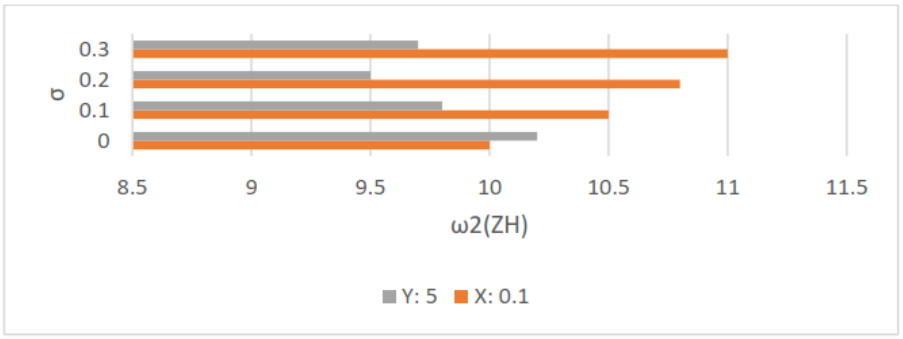

(b) Noise robustness of mode 2

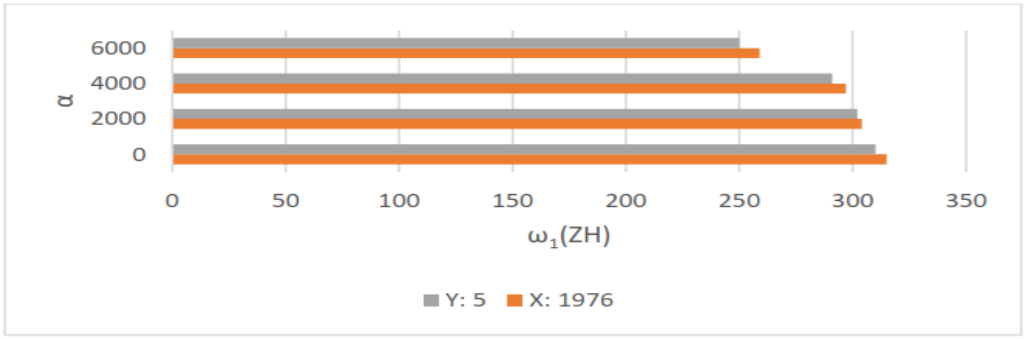

(c) Value robustness of mode 1

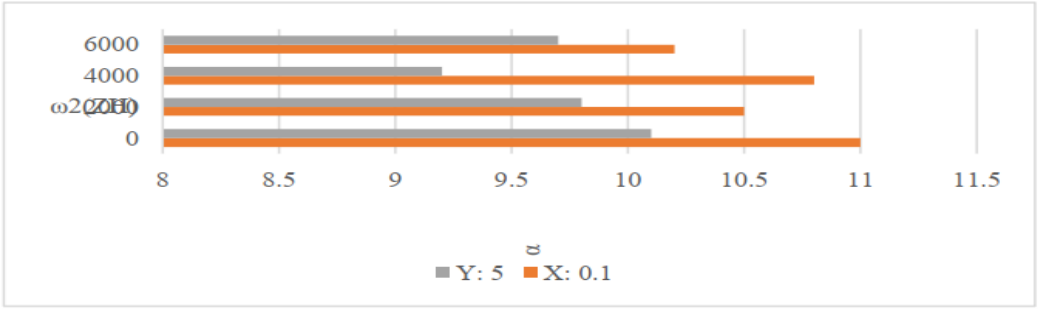

(d) Value robustness of mode 2

Figure 3: Noise Robustness and α Value Robustness of $X_1(t)$ Decomposition

Received: August 02, 2025

International Journal of Applied Mathematics
Volume 38 No. 8s, 2025
ISSN: 1311-1728 (printed version); ISSN: 1314-8060 (on-line version)

3.3 Comparative Study with Typical Algorithms

To further verify the decomposition effectiveness of the SAMMD algorithm, it is compared with classical multivariate signal decomposition methods such as MMD, MEMD, and FMEMD. The parameters involved in the above algorithms all use default values [5,9,13]. The above four algorithms are used to decompose the signal $X_1(t)$ (where the standard deviation of noise is set to 0.1). Here, to perform a quantitative comparison, the Sum of the Absolute Difference (SAD) is introduced to accurately measure the decomposition performance, defined as:

$$\mathrm{SAD} = \sum_{c=1}^{C} \sum_{\rho=1}^{K} \sum_{n=1}^{N} \left| x_{c,\rho}(n) - v_{c,\rho}(n) \right| \tag{13}$$

where $x_{c,\rho}(n)$ and $v_{c,\rho}(n)$ represent the k-th true mode and the decomposed mode, respectively. K, C, and N are the number of modes, the number of channels, and the data length, respectively.

The smaller the SAD value corresponding to the algorithm, the better the decomposition effect. The SAD values of the four algorithms when decomposing signal $X_1(t)$ are shown in Table 1. Compared with MMD, MEMD, and FMEMD, the proposed SAMMD algorithm has the smallest decomposition error and the highest decomposition accuracy.

Table 1. SAD values of four algorithms

Algorithm	SAD
MMD	845.56
MEMD	850.25
FMEMD	994.78
SAMMD	254.45

IV. Result Discussion

4.1 EEG Alpha Rhythm Extraction

This section demonstrates the efficacy of the proposed SAMMD method in signal decomposition and time-frequency analysis applications using a real-world case study. The actual case pertains to a collection of 4-channel electroencephalogram (EEG) recordings obtained from an experiment in which the individual sustained a condition of eyes-closed relaxation [5]. It has been established that, in a condition of closed eyes and relaxation, an alpha rhythm within the frequency range of 8–12 Hz can be observed in the EEG signal. Figure 4(a) illustrates the time-domain representation of the aforementioned EEG data, alongside the time-domain representations of the modes decomposed via SAMMD and their respective power spectral density (PSD) plots. In accordance with reference [5], only modes u_2, u_3, and u_5 are presented here. Figure 4(b) illustrates that the alpha rhythm in the EEG data is found in the mode u_2 derived from the SAMMD decomposition. All channels associated with u_2 exhibit the alpha rhythm, so confirming the mode alignment capacity of SAMMD in the processing of real signals. This outcome aligns with the decomposition findings of MMD, further validating the efficacy of the suggested algorithm. It is important to highlight that mode u_5, derived from both methods, is an artifact induced by the AC power supply, exhibiting a frequency of roughly 50 Hz [1,5]. The power frequency identified by MMD is around 40 Hz, which does not align with the real value [5]. Conversely, SAMMD accurately recovered this power frequency, as illustrated in Figure 4(b). This paper's proposed SAMMD shown superior performance in this real-world scenario.

Received: August 02, 2025

International Journal of Applied Mathematics
Volume 38 No. 8s, 2025
ISSN: 1311-1728 (printed version); ISSN: 1314-8060 (on-line version)

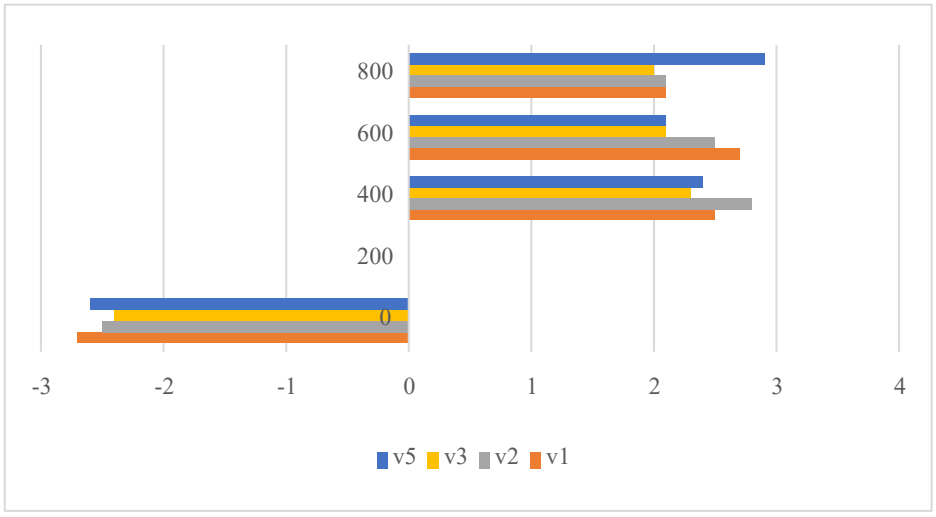

(a) SAMMD decomposition mode time domain diagram

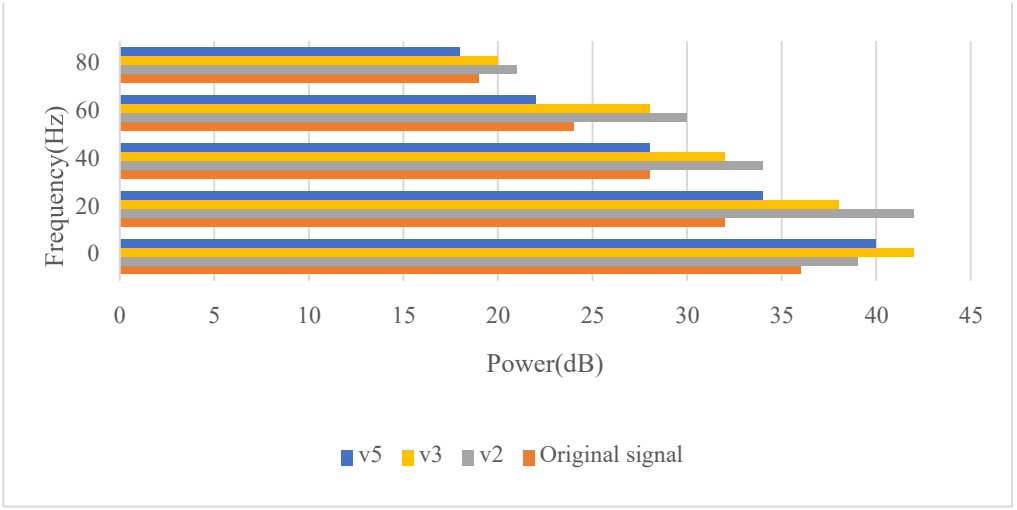

(b) SAMMD decomposition modal frequency domain diagram
Figure 4: Results of SAMMD decomposition of EEG signals

4.2 Plant-wide Oscillation Analysis in Control Systems

Oscillation is one of the most common anomalies in process control systems. Although oscillation usually originates in one source loop, it often propagates through interconnected loops, causing plant-wide oscillations. This can lead to wastage of production resources, product quality fluctuations, and even jeopardize the stability and safety of the system [24,25]. Therefore, detecting and analysing plant-wide oscillations is very necessary.

Here, SAMMD is applied to a plant-wide oscillation dataset observed in the flotation circuit of a mineral processing plant [26]. The flotation circuit consists of two parallel banks, each containing seven flotation cells in series (Bank 1: FT001 to FT007; Bank 2: FT008 to FT014). The data sampling interval is 10 seconds. For ease of display and analysis, nine units (i.e., FT002 to FT010) were selected here and labelled as variables $\mathbf{x}_1$ to $\mathbf{x}_9$. The first row of Figure 5 shows the measurements of the nine variables, and the remaining two rows show the SAMMD decomposed modes (u_1 , u_2).

Received: August 02, 2025

International Journal of Applied Mathematics
Volume 38 No. 8s, 2025
ISSN: 1311-1728 (printed version); ISSN: 1314-8060 (on-line version)

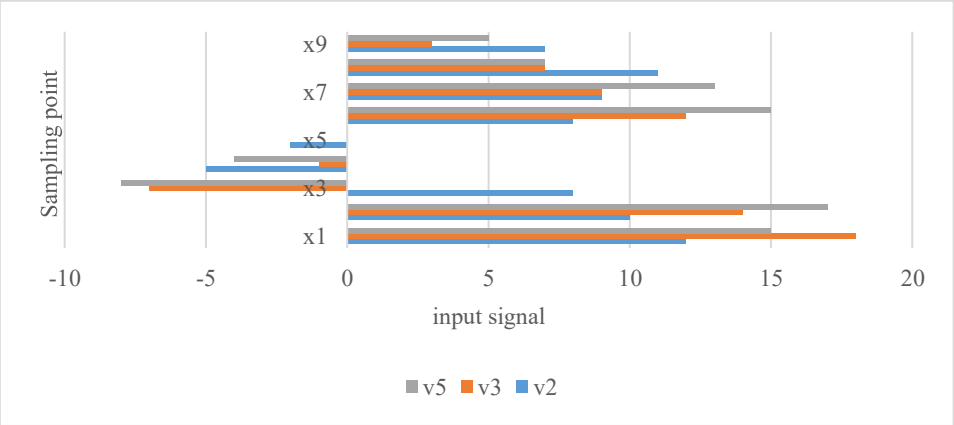

Figure 5: Plant-level oscillation data and decomposition results of SAMMD

Following reference [27], this paper adopts two indicators — the normalized correlation coefficient and the Sparsity Index (SI) — to detect oscillations in the modes. The normalized correlation coefficient (Equation 14) can eliminate false modes caused by mode alignment [24].

$$\theta_{\rho,c} = \frac{\rho_{\rho,c}}{\max\{\rho_{1,c},\rho_{2,c},\cdots,\rho_{K,c}\}} \tag{14}$$

Where $\rho_{\rho,c}$ is the correlation coefficient between the mode $v_{\rho,c}$ and the signal x_c. Only the modes with $\theta_{\rho,c} > T_\theta$ are retained for oscillation analysis, where the threshold is generally set as $T_\theta = 0.5$[27].

The calculation formula of the Sparsity Index is as follows:

$$\mathrm{SI} = \frac{\sqrt{N} - \left(\sum_{n=1}^{N} |\hat{v}_{\rho,c}^{n}| / \sqrt{\sum_{n=1}^{N} |\hat{v}_{\rho,c}^{n}|}\right)}{\sqrt{N} - 1} \tag{15}$$

Where $v_{\rho,c}^{\wedge}$ is the Fourier transform of the signal $v_{\rho,c}$ to be detected, and N denotes the length of the signal. Oscillatory modes exhibit distinct peaks in the frequency domain, with corresponding SI values close to 1.

According to [28], modes with SI values greater than 0.58 can be identified as oscillatory. We visualized the oscillation detection results of the modes decomposed by SAMMD, as shown in Figure 6, where black squares correspond to oscillatory modes and white squares correspond to non-oscillatory modes. It can be seen that mode v_2 in channels $x_1 \sim x_6$ exhibits an oscillation component of the same frequency, while mode v_1 in channels $x_7 \sim x_9$ contains an oscillation component of the same frequency. This is consistent with the analysis results of previous work [26]. The successful application of SAMMD in this plant-wide oscillation case further verifies the practicality and effectiveness of the proposed algorithm.

Received: August 02, 2025

International Journal of Applied Mathematics
Volume 38 No. 8s, 2025
ISSN: 1311-1728 (printed version); ISSN: 1314-8060 (on-line version)

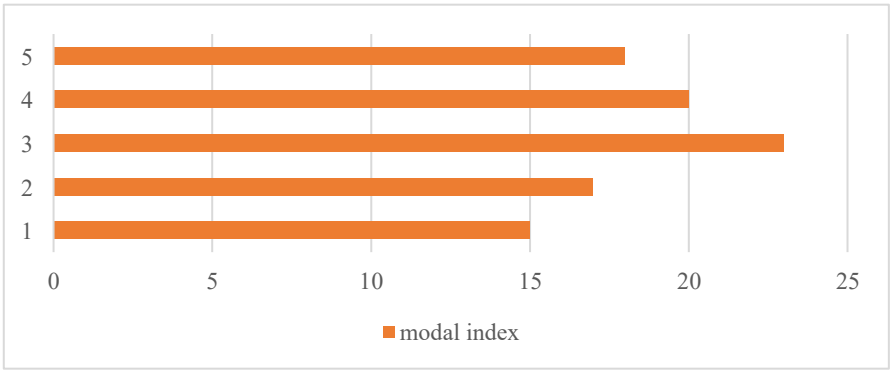

Figure 6: Visualization of plant-level oscillation detection results based on SAMMD

V. Conclusion

This paper proposed a self-adaptive multivariate variation mode decomposition (SAMMD) algorithm. The method adopts the idea of matching pursuit, using the energy proportion of the residual signal and the orthogonality of modes in the frequency domain to adaptively update the number of modes and the penalty factor α, thus solving the issue in the original MMD algorithm where parameters and α need to be present. Through representative simulations and real-world cases, it has been verified that the sub-signals decomposed by the proposed algorithm possess mode alignment (mode consistency), and it has demonstrated the effectiveness and superiority of the algorithm compared to other classical multivariate signal decomposition methods. The algorithm presented in this paper showed significant advantages in the analysis of multi-channel EEG signals and plant-wide oscillation signals in control systems. Future research will further explore the application of the SAMMD algorithm in other engineering fields. At the same time, drawing on the ideas of FMEMD, efforts can be made to transform the multivariate optimization problem in MMD into a univariate problem to improve the decomposition speed of the algorithm and address the challenge of MMD in handling multivariate signals with a large number of channels.

References

1. Yadav, D., Yadav, S., Veer, K., 2020. A comprehensive assessment of Brain–Computer Interfaces: Recent trends and challenges. *Journal of Neuroscience Methods*, 346, 108918. https://doi.org/10.1016/j.jneumeth.2020.108918.
2. Wu, H., Hu, X., Zeng, Y., 2024. A fast dynamic causal modeling regression method for fMRI. *NeuroImage*, 304, 120954. https://doi.org/10.1016/j.neuroimage.2024.120954.
3. Boashash, B. (Ed.), 2016. Time–Frequency Methodologies in Neurosciences. In: *Time–Frequency Signal Analysis and Processing* (2nd ed.). Academic Press, pp. 915–966. https://doi.org/10.1016/B978-0-12-398499-9.00016-9.
4. McDonough, I.M., Madan, C.R., 2021. Structural complexity is negatively associated with brain activity: a novel multimodal test of compensation theories of aging. *Neurobiology of Aging*, 98, 185–196. https://doi.org/10.1016/j.neurobiolaging.2020.10.023.
5. Fein, G., Cardenas, V., 2019. Brain networks in active alcoholism and enduring recovery: functional magnetic resonance imaging, electrophysiological studies, and implications for targeted treatments. In: Preedy, V.R. (Ed.), *Neuroscience of Alcohol*. Academic Press, pp. 237–247. https://doi.org/10.1016/B978-0-12-813125-1.00025-8.
6. Toma, F.-M., 2023. A hybrid neuro-experimental decision support system to classify overconfidence and performance in a simulated bubble using a passive BCI. *Expert Systems with Applications*, 212, 118722. https://doi.org/10.1016/j.eswa.2022.118722.
7. Ji, P., Ye, J., Mu, Y., Lin, W., Tian, Y., Hens, C., Perc, M., Tang, Y., Sun, J., Kurths, J., 2023. Signal propagation in complex networks. *Physics Reports*, 1017, 1–96. https://doi.org/10.1016/j.physrep.2023.03.005.

Received: August 02, 2025

ISSN: 1311-1728 (printed version); ISSN: 1314-8060 (on-line version)

8. Duff, E.P., Moultrie, F., van der Vaart, M., Goksan, S., Abos, A., Fitzgibbon, S.P., Baxter, L., Wager, T.D., Slater, R., 2020. Inferring pain experience in infants using quantitative whole-brain functional MRI signatures: a cross-sectional, observational study. *The Lancet Digital Health*, 2(9), e458–e467. https://doi.org/10.1016/S2589-7500(20)30168-0.
9. Yang, D., Geng, D., Zheng, L., Cai, M., Hao, W., 2021. Entropy-based analysis and classification of acute tonic pain from microwave transcranial signals obtained via the microwave-scattering approach. *Biomedical Signal Processing and Control*, 65, 102391. https://doi.org/10.1016/j.bspc.2020.102391.
10. Naik, R., Chaudhari, K., Jadhav, K., Joshi, A., 2025. MindCeive: Perceiving human imagination using CNN–GRU and GANs. *Biomedical Signal Processing and Control*, 100 (Part C), 107110. https://doi.org/10.1016/j.bspc.2024.107110.
11. Grady, C.L., Garrett, D.D., 2018. Brain signal variability is modulated as a function of internal and external demand in younger and older adults. *NeuroImage*, 169, 510–523. https://doi.org/10.1016/j.neuroimage.2017.12.031.
12. Zhou, Z., Cai, B., Zhang, G., Zhang, A., Calhoun, V.D., Wang, Y.-P., 2020. Prediction and classification of sleep quality based on phase synchronization related whole-brain dynamic connectivity using resting-state fMRI. *NeuroImage*, 221, 117190. https://doi.org/10.1016/j.neuroimage.2020.117190.
13. Jeyakumar, V., Krishnan, P.T., Sundaram, P., Raj, A.N.J., 2022. Brain–computer interface in Internet of Things environment. In: Bhoi, A.K., de Albuquerque, V.H.C., Sur, S.N., Barsocchi, P. (Eds.), *Intelligent Data-Centric Systems: 5G IoT and Edge Computing for Smart Healthcare*. Academic Press, pp. 231–255. https://doi.org/10.1016/B978-0-323-90548-0.00012-7.
14. Chapter 9 - Brain–computer interface in Internet of Things environment. In: Bhoi, A.K., de Albuquerque, V.H.C., Sur, S.N., Barsocchi, P. (Eds.), *Intelligent Data-Centric Systems: 5G IoT and Edge Computing for Smart Healthcare*. Academic Press, 2022, pp. 231–255. https://doi.org/10.1016/B978-0-323-90548-0.00012-7.
15. Bhoi, A.K., de Albuquerque, V.H.C., Sur, S.N., Barsocchi, P. (Eds.), 2022. *Intelligent Data-Centric Systems: 5G IoT and Edge Computing for Smart Healthcare*. Academic Press. ISBN 9780323905480. https://doi.org/10.1016/B978-0-323-90548-0.00012-7.
16. Al-Baddai, S., Al-Subari, K., Tomé, A.M., Volberg, G., Hanslmayr, S., Hammwöhner, R., Lang, E.W., 2014. Bidimensional ensemble empirical mode decomposition of functional biomedical images taken during a contour integration task. *Biomedical Signal Processing and Control*, 13, 218–236. https://doi.org/10.1016/j.bspc.2014.04.011.
17. Esfahlani, F.Z., Jo, Y., Puxeddu, M.G., Merritt, H., Tanner, J.C., Greenwell, S., Patel, R., Faskowitz, J., Betzel, R.F., 2021. Modularity maximization as a flexible and generic framework for brain network exploratory analysis. *NeuroImage*, 244, 118607. https://doi.org/10.1016/j.neuroimage.2021.118607.
18. Alam, M.S.B., Lameesa, A., Sharmin, S., Afrin, S., Ahmed, S.F., Nikoo, M.R., Gandomi, A.H., 2025. Role of deep learning in cognitive healthcare: wearable signal analysis, algorithms, benefits, and challenges. *Digital Communications and Networks*, (2025). https://doi.org/10.1016/j.dcan.2025.04.001.
19. Hramov, A.E., Maksimenko, V.A., Pisarchik, A.N., 2021. Physical principles of brain–computer interfaces and their applications for rehabilitation, robotics and control of human brain states. *Physics Reports*, 918, 1–133. https://doi.org/10.1016/j.physrep.2021.03.002.
20. Isufi, E., Leus, G., Beferull-Lozano, B., Barbarossa, S., Di Lorenzo, P., 2025. Topological signal processing and learning: Recent advances and future challenges. *Signal Processing*, 233, 109930. https://doi.org/10.1016/j.sigpro.2025.109930.

Received: August 02, 2025

ISSN: 1311-1728 (printed version); ISSN: 1314-8060 (on-line version)

21. Zhang, S., Zhang, H., Wang, C., Lin, H., 2024. Bionic modeling and dynamics analysis of heterogeneous brain regions connected by memristive synaptic crosstalk. *Chaos, Solitons & Fractals*, 179, 114459. https://doi.org/10.1016/j.chaos.2024.114459.
22. Fruehlinger, C., Paul, K., Wacker, J., 2024. Can personality traits be predicted from resting-state EEG oscillations? A replication study. *Biological Psychology*, 193, 108955. https://doi.org/10.1016/j.biopsycho.2024.108955.
23. Dogan, S., Tuncer, T., Barua, P.D., Acharya, U.R., 2024. Automated EEG-based language detection using directed quantum pattern technique. *Applied Soft Computing*, 167 (Part A), 112301. https://doi.org/10.1016/j.asoc.2024.112301.
24. Papo, D., Buldú, J.M., 2024. Does the brain behave like a (complex) network? I. Dynamics. *Physics of Life Reviews*, 48, 47–98. https://doi.org/10.1016/j.plrev.2023.12.006.
25. Kaur, C., Bisht, A., Singh, P., Joshi, G., 2021. EEG signal denoising using a hybrid approach of Variational Mode Decomposition and wavelets for depression. *Biomedical Signal Processing and Control*, 65, 102337. https://doi.org/10.1016/j.bspc.2020.102337.
26. Kardam, V.S., Taran, S., Pandey, A., 2023. Motor imagery tasks based electroencephalogram signals classification using data-driven features. *Neuroscience Informatics*, 3(2), 100128. https://doi.org/10.1016/j.neuri.2023.100128.
27. Betzel, R.F., Faskowitz, J., Sporns, O., 2023. Living on the edge: network neuroscience beyond nodes. *Trends in Cognitive Sciences*, 27(11), 1068–1084. https://doi.org/10.1016/j.tics.2023.08.009.
28. Hu, G., Li, H., Zhao, W., Hao, Y., Bai, Z., Nickerson, L.D., Cong, F., 2022. Discovering hidden brain network responses to naturalistic stimuli via tensor component analysis of multi-subject fMRI data. *NeuroImage*, 255, 119193. https://doi.org/10.1016/j.neuroimage.2022.119193.
29. Stecher, R., Cichy, R.M., Kaiser, D., 2025. Decoding the rhythmic representation and communication of visual contents. *Trends in Neurosciences*, 48(3), 178–188. https://doi.org/10.1016/j.tins.2024.12.005.
30. Paillard, J., Hipp, J.F., Engemann, D.A., 2025. GREEN: A lightweight architecture using learnable wavelets and Riemannian geometry for biomarker exploration with EEG signals. *Patterns*, 6(3), 101182. https://doi.org/10.1016/j.patter.2025.101182.
31. Lin, S.-H.N., Lin, G.-H., Tsai, P.-J., Hsu, A.-L., Lo, M.-T., Yang, A.C., Lin, C.-P., Wu, C.-W., 2016. Sensitivity enhancement of task-evoked fMRI using ensemble empirical mode decomposition. *Journal of Neuroscience Methods*, 258, 56–66. https://doi.org/10.1016/j.jneumeth.2015.10.009.
32. Prakash, R.S., Shankar, A., Tripathi, V., Yang, W.F.Z., Fisher, M., Bauer, C.C.C., Betzel, R., Sacchet, M.D., 2025. Mindfulness meditation and network neuroscience: review, synthesis, and future directions. *Biological Psychiatry: Cognitive Neuroscience and Neuroimaging*, 10(4), 350–358. https://doi.org/10.1016/j.bpsc.2024.11.005.
33. Sirpal, P., Sikora, W.A., Refai, H.H., 2025. Multimodal sleep signal tensor decomposition and hidden Markov modeling for temazepam-induced anomalies across age groups. *Journal of Neuroscience Methods*, 416, 110375. https://doi.org/10.1016/j.jneumeth.2025.110375.
34. Yang, L., Qiao, C., Kanamori, T., Calhoun, V.D., Stephen, J.M., Wilson, T.W., Wang, Y.-P., 2025. Tensor dictionary-based heterogeneous transfer learning to study emotion-related gender differences in brain. *Neural Networks*, 183, 106974. https://doi.org/10.1016/j.neunet.2024.106974.
35. Chen, L., Qiao, C., Ren, K., Qu, G., Calhoun, V.D., Stephen, J.M., Wilson, T.W., Wang, Y.-P., 2024. Explainable spatio-temporal graph evolution learning with applications to dynamic brain network analysis during development. *NeuroImage*, 298, 120771. https://doi.org/10.1016/j.neuroimage.2024.120771.

Received: August 02, 2025

ISSN: 1311-1728 (printed version); ISSN: 1314-8060 (on-line version)

36. Zuo, Q., Di, Y., Ye, C., Shi, B., Chen, J., Wei, H., Li, R., Lei, B., 2025. Bidirectional generative diffusion model with cascaded symmetric attention for brain connectivity-to-connectivity translation. *Biomedical Signal Processing and Control*, 108, 107900. https://doi.org/10.1016/j.bspc.2025.107900.
37. Wang, F., Ke, H., Tang, Y., 2025. Fusion of generative adversarial networks and non-negative tensor decomposition for depression fMRI data analysis. *Information Processing & Management*, 62(2), 103961. https://doi.org/10.1016/j.ipm.2024.103961.
38. Das, K., Mondal, A., Phukan, N., Pachori, R.B., 2025. Multivariate adaptive signal decomposition techniques and their applications to EEG signal processing: An introduction. In: El-Baz, A.S., Suri, J.S. (Eds.), *Advances in Neural Engineering: Signal Processing Strategies*. Academic Press, pp. 137–161. https://doi.org/10.1016/B978-0-323-95437-2.00011-2.
39. Du, X., Xi, M., Ding, X., Wang, F., Qiu, S., Lv, Y., Liu, Q., 2025. Motor imagery EEG signal classification based on deformable convolution v3 and adaptive spatial attention mechanism. *Biomedical Signal Processing and Control*, 99, 106905. https://doi.org/10.1016/j.bspc.2024.106905.
40. Jafari, M., Shoeibi, A., Khodatars, M., Bagherzadeh, S., Shalbaf, A., López García, D., Gorriz, J.M., Acharya, U.R., 2023. Emotion recognition in EEG signals using deep learning methods: a review. *Computers in Biology and Medicine*, 165, 107450. https://doi.org/10.1016/j.compbiomed.2023.107450.

Received: August 02, 2025